Infrared and UV-visible spectral data show that NO is lost from $[(TPP)Co(NO)]^-$ and that the generated $[(TPP)Co]^-$ reacts with the CH_2Cl_2 solvent to give $(TPP)Co(CH_2Cl)$. This reaction has been discussed for the reduction of $(TPP)Co$[27] in CH_2Cl_2, and a similar sequence of steps occurs after reduction of (TPP)Co(NO) in CH_2Cl_2. The overall conversion of (TPP)Co(NO) to $(TPP)Co(CH_2Cl)$ is given by eq 3, 8, and 9. Similar reactions have

$$[(TPP)Co(NO)]^- \rightarrow [(TPP)Co]^- + NO \quad (8)$$

$$[(TPP)Co]^- + CH_2Cl_2 \rightarrow (TPP)Co(CH_2Cl) + Cl^- \quad (9)$$

also been observed between electrochemically generated $[(TPP)Co]^-$ and alkyl or aryl halides.[28]

Additional proof for the sequence of steps given in reactions 8 and 9 comes from thin-layer spectroelectrochemistry. Spectral changes monitored during controlled-potential reduction of (TPP)Co(NO) are shown in Figure 6. The final spectrum is identical with the UV-visible spectrum of genuine $(TPP)Co(CH_2Cl)$ as well as with other σ-bonded (TPP)Co(R) complexes in CH_2Cl_2.[27-29]

Finally, the difference FTIR spectrum after reduction of (TPP)Co(NO) at -1.30 V shows a negative peak at 1684 cm^{-1}, and no characteristic positive band for NO-containing species was observed. This also indicates that NO dissociation has occurred after the first reduction.

In summary, the oxidations and reductions of (TPP)Co(NO) are reversible at a microelectrode, but the ultimate products are not always those shown by eq 1-5. This is due to the extreme reactivity of the singly reduced and doubly oxidized species. It is anticipated that several additional NO complexes may be sufficiently stabilized to be spectroscopically characterized at low temperature, and studies are now being carried out along these lines.

Acknowledgment. The support of the National Science Foundation (Grant CHE-8515411) is gratefully acknowledged.

Registry No. (TPP)Co(NO), 42034-08-2; CH_2Cl_2, 75-09-2; Pt, 7440-06-4; (TPP)Co, 14172-90-8.

(27) Kadish, K. M.; Lin, X. Q.; Han, B. C. *Inorg. Chem.* **1987**, *26*, 4161.
(28) Guilard, R.; Lecomte, C.; Kadish, K. M. *Struct. Bonding (Berlin)* **1987**, *64*, 206-268.
(29) Dolphin, D.; Halko, D. J.; Johnson, E. *Inorg. Chem.* **1981**, *20*, 4384.

Contribution from the Department of Chemistry, Indian Institute of Technology, Madras, India

Spectroscopic Investigation of Intermolecular Interactions in Dithiolate Complexes of Nickel

S. Lalitha, G. V. R. Chandramouli, and P. T. Manoharan*

Received May 27, 1987

A spectroscopic study on maleonitriledithiolato complexes of the type $R_n[M(mnt)_2]$, where n = 1 or 2, M = Ni(II) or Ni(III), and R = $(CH_3)_4N$ or $(n\text{-}C_4H_9)_4N$, is presented. On the basis of the charge potential model, with incorporation of electronegativities, the charges on the various atoms have been calculated by using the binding energies obtained from photoelectron spectroscopic experiments. These are found to compare well with those reported by Xα calculations. The binding energy shifts of the atoms on $[(n\text{-}C_4H_9)_4N]_2[Ni(mnt)_2]$ are observed to follow a different trend compared with that in the other three complexes. This difference in the charge distribution in the diamagnetic complex with tetrabutylammonium as the cation has been explained with the help of molecular projections. It has been inferred that there is an interaction between the cation and the complex anion in this case. EPR and Raman spectral studies on this complex at low temperatures (down to 20 K) are reported here. Two phase transitions, which also involve a slight molecular distortion, are detected at 50 and 20 K. Infrared spectra of all these complexes are compared, and this also reveals the same anomalous trend. In order to ascertain this behavior, single-crystal electronic spectra of $[(CH_3)_4N]_2[Ni(mnt)_2]$ at various temperatures are reported.

Introduction

The remarkable oxidation-reduction behavior of metal dithiolene compounds has generated an intense interest in the synthetic, spectroscopic, and theoretical aspects of these compounds.[1-6] Apart from the interest in these compounds from a purely academic point of view, these systems are now widely employed in industries.[2] One such system widely studied is the maleonitriledithiolate (mnt) complex of transition metals.[3-6] Some of these complexes are, for example, used as an autooxidation catalyst[7] and as a catalyst for the photochemical decomposition of water.[8] A recent paper reports the photoelectrochemical study of some of these complexes.[9]

We have chosen to investigate complexes of the type $R_n^+[M(mnt)_2]^{n-}$, where M = Ni(II), Ni(III), Co(II), Co(III), and Cu(II) and R = $[N(CH_3)_4]$, $[N(C_4H_9)_4]$ (referred to hereafter as Me_4N and $n\text{-}Bu_4N$ respectively), *N*-methylphenazinium, tropilium, etc. by photoelectron spectroscopy, EPR, Raman, optical, and IR spectroscopic techniques. In this paper we present the results pertaining to our study on $R_n^+[Ni(mnt)_2]^{n-}$ complexes, where R = $[N(CH_3)_4]$ and $[N(C_4H_9)_4]$, n = 1 and 2, and M = Ni(II) or Ni(III) in which the complex anion has a planar geometry as shown in Figure 1.

X-ray photoelectron spectroscopy enables a fresh insight into this fairly complex bonding system, since the binding energy (BE) of the core levels of all the atoms can easily be measured and the charges on these atomic sites can be determined. While the BE

(1) McCleverty, J. A. *Prog. Inorg. Chem.* **1968**, *10*, 49.
(2) Burns, R. P.; McAuliff, C. A. *Adv. Inorg. Chem. Radiochem.* **1979**, *22*, 303.
(3) Shupack, S. I.; Billig, E.; Clark, R. J. H.; Williams, R.; Gray, H. B. *J. Am. Chem. Soc.* **1964**, *86*, 4594.
(4) Schrauzer, G. N.; Mayweg, V. P. *J. Am. Chem. Soc.* **1965**, *87*, 3585.
(5) Schmitt, R. D.; Maki, A. H. *J. Am. Chem. Soc.* **1968**, *90*, 2288.
(6) Sano, M.; Adachi, H.; Yamatera, H. *Bull. Chem. Soc. Jpn.* **1981**, *54*, 2636.
(7) Sultin, N.; Yandell, Y. K. *J. Am. Chem. Soc.* **1973**, *95*, 4847.
(8) Henning, R.; Schlamann, W.; Kirsh, H. *Angew. Chem.* **1980**, *92*, 664.
(9) Persaud, L.; Langford, C. H. *Inorg. Chem.* **1985**, *24*, 3562.

0020-1669/88/1327-1492$01.50/0

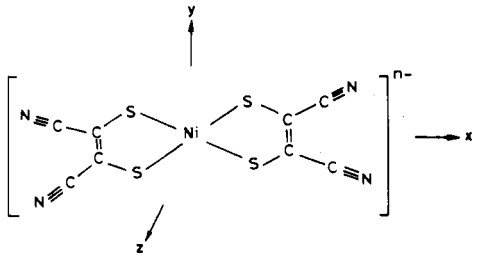

Figure 1. Molecular structure of $[Ni(mnt)_2]^{n-}$ along with the coordinate system.

of the electrons in the valence levels are greatly affected by bond formation, the BE of the electrons in the core levels are affected more by a change in the potential caused by the valence electrons. The shift in the BE of core electrons due to change in the potential, in general, can vary in the range 0.2–8.0 eV with variation in the charge density at that particular atomic site. The binding energy shifts reflect not only on the charge on a particular atom but also on the charges on the neighboring atoms.[10] Hence a careful study of these binding energy shifts in a molecule can reveal inter- and intramolecular interactions. There have been a few reports on the ESCA study of mnt complexes of transition metals,[6,11,12] which did not go into the depth of interaction of neighboring atoms. Recently there has been an interesting report on the optical spectrum of $[n\text{-}Bu_4N]_2[Ni(mnt)_2]$, which exhibits an anomalous behavior.[13] Our ESCA studies on this system not only extract the reason for such an observation but also explain the influence of the cation on the complex moiety. It was observed that the binding energy shifts in the metal depend upon the electronegativities of the ligands.[12] However, no attempt has been made to rationalize this effect. Therefore, in this paper we have developed an equation to account for the effect of the neighboring atomic charges and their electronegativities on the binding energies of core electrons of each atom. Further, in support of our ESCA studies, infrared spectral studies have been made. Consolidating the data thus obtained, we predict molecular and crystal distortions in $[n\text{-}Bu_4N]_2[Ni(mnt)_2]$ at low temperatures. In support of this, EPR and Raman spectral studies have been carried out on the above complex.

Experimental Section

The sodium salt of maleonitriledithiolate was prepared,[14] and the complexes of Ni(II), Cu(II), and Ni(III) were then prepared by standard methods.[15] Single crystals of the above complexes were grown by slow evaporation of their solution in acetone. XPS spectra were recorded on a VG Mark II ESCA spectrometer equipped with a twin anode of Al and Mg. The resolution in this instrument is 0.2 eV. Samples were well powdered and packed tightly on Ni stubs, and a spot of silver paint was placed on the sample. The Ag(3d) (368.2, 374.2 eV) levels were used as a standard since the C(1s) generally used as a standard (in compounds containing alkyl groups) could not be well resolved from that arising from the cyano as well as the olefinic carbon peaks. Moreover, the use of silver paint permits a common standard in the study of all complexes including those in which an alkyl carbon atom may be absent.[16] All measurements were made at room temperature of 25 °C and at 10^{-9} Torr pressure. Samples were studied by using Mg Kα, and satellites due to the nonmonochromatic source were subtracted. Further, the raw data were corrected for the experimental broadening functions by using a Fourier deconvolution program,[17] thereby, an enhanced resolution was obtained. The C(1s) peaks corresponding to the different types of C atoms were obtained by using a Gaussian bandfit program.[18] IR spectra of the complexes in the form of KBr pellet were measured on a PE983 infrared spectrophotometer. The peak positions were accurately identified by using a microcomputer attached to the spectrophotometer. Optical spectral measurements were made on a single crystal of $[Me_4N]_2[Ni(mnt)_2]$ as a function of temperature by using a Cary 2300 UV–vis–near-IR spectrophotometer. EPR spectra of 1% copper(II) doped $[n\text{-}Bu_4N]_2[Ni(mnt)_2]$ were measured on a Varian E-4 spectrometer at X-band frequency. Single-crystal Raman spectral measurements were made on a Varian Cary 82 Raman spectrophotometer. The 6471-Å line of a krypton laser was used with 50 mW of power for excitation. All the low-temperature measurements were made by using a CTI Cryogenics cryodyne cryocooler. All of the experiments were repeated for reproducibility.

Method of Investigation

The charges on the atoms are generally obtained by semiempirical charge potential model[10] and MO calculations. MO calculations (other than Xα) are usually inadequate to explain the binding energies of an ESCA spectrum since they do not consider the relaxation effects that occur during the ejection of electrons. According to the charge potential model

$$E_j = E_j^\circ + kq_j^v + V \tag{1}$$

i.e.

$$\Delta E_j = kq_j + V \tag{2}$$

where E_j is the BE for a given core level of an atom j in a molecule, E_j° is the BE of the same core level of the same atom when the charge is zero and q_j^v is the charge on the atom j due to the valence orbitals, which can be approximated to q_j itself.[10] V is the potential contributed by the other atoms due to their charge q_l at a distance R_{jl} from the atom j, and it is defined as $V = \sum_{l \neq j} q_l e^2/R_{jl}$. k is determined as the average of the expectation values of $1/r$ over all the valence orbitals of atom j, i.e. $\langle 1/r \rangle_j^v$. Since ΔE_j is in eV and both R_{jl} and $\langle 1/r \rangle_j^v$ are in au, the terms on the right-hand side should be multiplied by 27.2 for the units to be in eV.

$$\therefore \quad \Delta E_j = 27.2\langle 1/r \rangle_j^v q_j + 27.2\ V \tag{3}$$

The charges calculated from (3) are found to be very low. Probably for this reason, Larsson[19] has tried to determine the k values by a study of large number of molecules. Though his equations give reasonable charges, they do not consider the effects of neighboring atoms. However, since the value of k is obtained from a plot of experimental BE and known charges, this estimate of k takes relaxation effects into account. Blomquist[11] obtains the charges on the iron dithiolate system from Larsson's k values. Hence, consolidating all the earlier methods, we have attempted to develop a simple emperical equation to obtain charges that is applicable to all our metal complexes in the solid state.

Since (3) is based on the initial state of the system, it assumes that the BE measured is before any relaxation of orbitals has occured. But in reality this is a drastic approximation. On the removal of a core electron by photoionization, the $\langle 1/r \rangle_j^v$ calculated on the basis of the initial state wave functions are no longer valid. The electrons of the valence level flow toward the core hole, and the extent of flow is more when the electronegativity, χ, is higher. Therefore this relation between electronegativity and orbital contraction is incorporated into (3) in order to take into account the change in $\langle 1/r \rangle_j^v$ due to relaxation. A similar argument can be extended for the correction in the value of R_{jl}. Comparing k values obtained from the modified version of (3) with empirically reported values of k by Larsson[19] for C, N, and S and by Grim[20] for nickel, we found that the parameter k of Larsson's equation is approximately equal to $(27.2/\chi_j)\langle 1/r \rangle_j^v$ where χ corresponds to Pauling's electronegativity. There has

(10) Carlson, T. A. *Photoelectron and Augerelectron Spectroscopy*; Plenum: New York, 1975.
(11) Blomquist, J.; Helgeson, U. *Chem. Phys.* **1983**, *76*, 71.
(12) Grim, S. O.; Matienzo, L. J.; Swartz, W. E., Jr. *J. Am. Chem. Soc.* **1972**, *94*, 5116.
(13) Chandramouli, G. V. R.; Manoharan, P. T. *Inorg. Chem.* **1986**, *25*, 4680.
(14) Bahr, G.; Schleitzer, G. *Chem. Ber.* **1957**, *90*, 438.
(15) Davisson, A.; Edelstein, N.; Holm, R. H.; Maki, A. H. *Inorg. Chem.* **1963**, *2*, 1227.
(16) As in the case where R = tropilium.
(17) Betham, N.; Orchard, A. F. *J. Electron Spectrosc. Relat. Phenom.* **1976**, *19*, 129.
(18) A Gaussian fitting program has been developed by us for use on a personal computer.
(19) Larsson, R. *J. Electron Spectrosc. Relat. Phenom.* **1981**, *24*, 37.
(20) Grim, S. O.; Matienzo, L. J.; Swartz, W. E., Jr. *Inorg. Chem.* **1974**, *13*, 447.

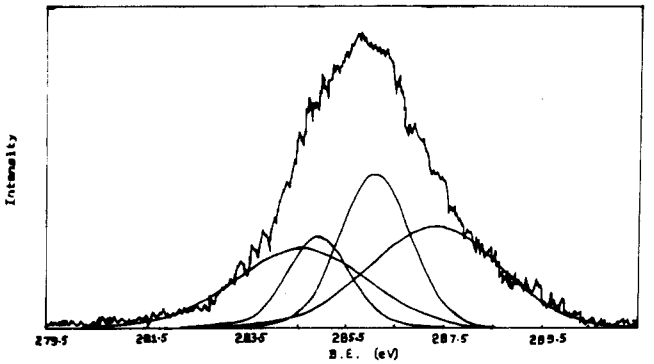

Figure 2. Photoelectron spectrum of $[Me_4N][Ni(mnt)_2]$ in the C(1s) region. Both the experimental spectrum and the individual bands fitted are shown.

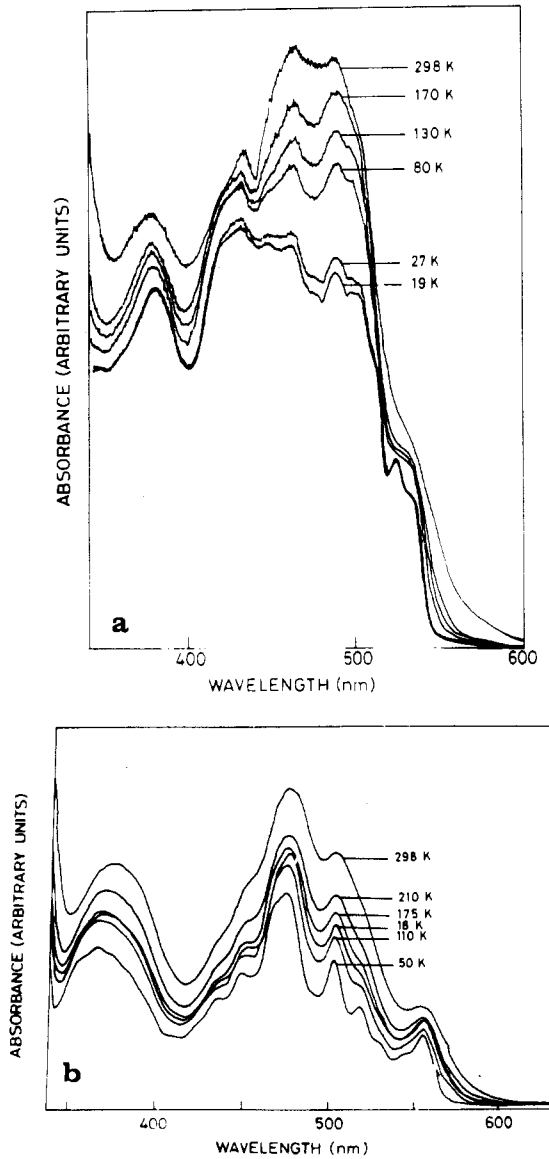

Figure 3. Single-crystal electronic spectra in the temperature range 18–298 K: (a) $[Me_4N]_2[Ni(mnt)_2]$; (b) $[n\text{-}Bu_4N]_2[Ni(mnt)_2]$.

been a report by Grim et al.[20] that the BE shifts of nickel depend on the electronegativity of the ligands. Considering all these aspects, we have modified (3) as

$$\Delta E_j = (27.2/\chi_j)q_j(1/r)_j^p + \sum_{j\neq l}(27.2/\chi_l)q_l/R_{jl} \quad (4)$$

A comparison of charges calculated by various methods is presented in the discussion section. Moreover, the charges calculated

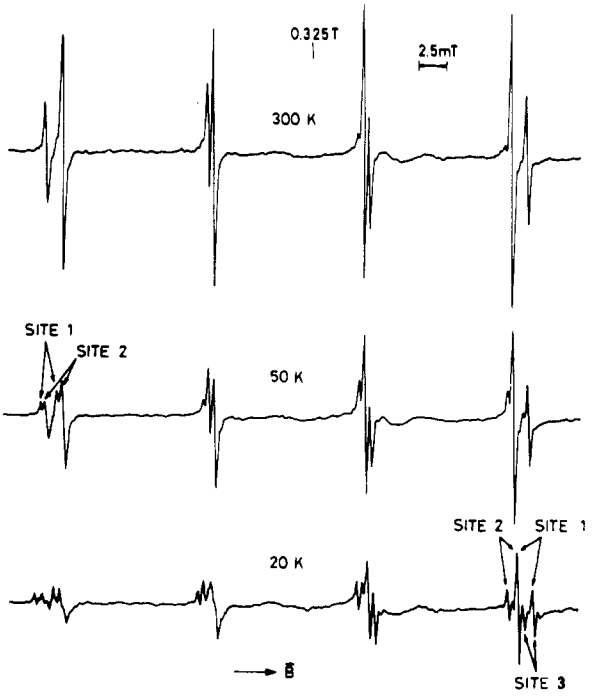

Figure 4. Temperature-dependent EPR spectrum of a single crystal of $[n\text{-}Bu_4N]_2[Cu(mnt)_2]$ doped in $[n\text{-}Bu_4N]_2[Ni(mnt)_2]$ in the range 20–300 K at X-band frequency.

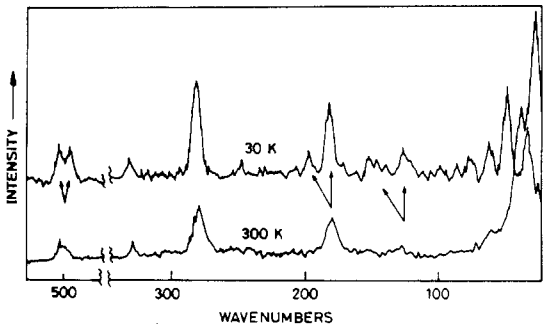

Figure 5. Raman spectra of a single crystal of $[n\text{-}Bu_4N]_2[Ni(mnt)_2]$ at 30 and 300 K.

by using this equation compare well with those obtained from $X\alpha$ calculation on the anionic moiety.[6]

Results

The observed ESCA spectra were initially corrected for the instrumental broadening, and the binding energies for $Ni(2p_{3/2})$, S(2p) and N(1s) were noted. However, the C(1s) signal appears as an overlap of several peaks, indicating the presence of different types of carbon atoms. These peaks were resolved by using a Gaussian deconvolution program. The C(1s) ESCA spectrum in the region 280–290 eV for $[Me_4N][Ni(mnt)_2]$ is shown in Figure 2. Both the raw data (after the correction for instrumental broadening factors) and the Gaussian fitted peaks of the different carbon atoms are shown. The fitting shown in Figure 2 for the C(1s) envelope was done with the following assumptions and constraints.

(a) The observed spectrum was corrected for instrumental broadening. Satellites due to the nonmonochromaticity of the X-ray source were subtracted. Background correction was also done.

(b) The number of bands and their positions were then estimated as follows.

(i) First, they were estimated from the number of chemically inequivalent carbon atoms based on the crystal structure as well as from $X\alpha$ calculation.[6] From the former, we assumed that there are four different types of carbon atoms in the $n\text{-}Bu_4N$ complexes (namely B and D) while there are three different types of carbon atoms in the Me_4N complexes (namely A and C) as shown in

Table I. Binding Energy Shifts (ΔE_j) in $R_n[Ni(mnt)_2]$ Complexes

	ΔE_j, eV							
			C(1s)				N(1s)	
compd	$Ni(2p_{3/2})$	S(2p)	C(1)	C(2)	C(3)	C(4)	N(1)	N(2)
$[Me_4N]_2[Ni(mnt)_2]$ (A)	3.2	−0.9	−0.4	2.8	1.4		−0.9	2.7
$[n\text{-}Bu_4N]_2[Ni(mnt)_2]$ (B)	3.6	0.1	0.1	2.8	1.9	1.0	−0.8	2.3
$[Me_4N][Ni(mnt)_2]$ (C)	3.5	−0.2	−0.2	2.8	1.4		−1.4	1.6
$[n\text{-}Bu_4N][Ni(mnt)_2]$ (D)	4.1	−0.2	−0.7	2.5	1.2	0.3	−1.4	2.0

Table II. Infrared Spectral Data for $R_n[Ni(mnt)_2]$ Complexes

	normal mode of vibration, cm^{-1}			
complex	ν(C—S) + ν(C—C)	ν(C=C)	π(C—CN)	ν(C≡N)
$[Me_4N]_2[Ni(mnt)_2]$ (A)	1060	1485	1107	2198
$[n\text{-}Bu_4N]_2[Ni(mnt)_2]$ (B)	1068	1481	1110	2195
$[Me_4N][Ni(mnt)_2]$ (C)	1060	1482	1111	2207
$[n\text{-}Bu_4N][Ni(mnt)_2]$ (D)	1050	1485	1106	2205

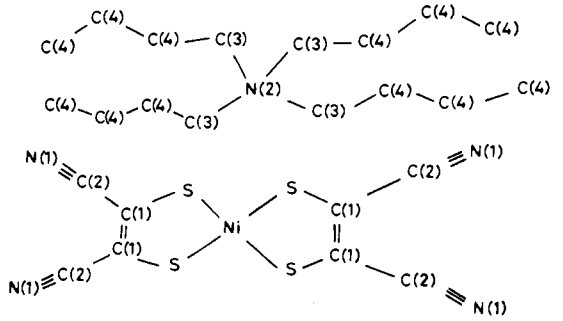

Figure 6. Labels of atoms in $[n\text{-}Bu_4N]_2[Ni(mnt)_2]$ based on their chemical equivalence used for the interpretation of ESCA results.

Figure 6. Xα calculations on the anionic moiety reveal a negative charge for the C(1) atoms and a positive chare for C(2). Comparing the electronic environment and the neighboring atoms for each type of carbon atom, we assumed that C(3) and C(4) have charges in between those of C(1) and C(2).

(ii) Another factor considered is that the relative area under the curve is proportional to the number of carbon atoms of each type present.

(iii) The pump oil C(1s) peak was fixed at 285 eV because in the standard sample of gold as well as in the empty nickel stub (referenced to Ag(3d)), the C(1s) peak from the pump oil appeared at 285 eV and its intensity is not negligible. (We have repeated the experiment several times.) This has been greatly minimized by maintaining a very low pressure of 10^{-9}–10^{-10} Torr.

(iv) Though there can be solutions with different intensities of bands, the peak positions remain at the same value. It is quite gratifying to note that the standard deviation between the experimental and the fitted spectra in all the complexes was about 0.02. The binding energy shifts (ΔE's) were calculated by taking the $E°$ values for $Ni(2p_{3/2})$, S(2p), C(1s), and N(1s) as 852.5, 164.8, 284.8, and 401.6, respectively,[21] which are presented in Table I. The infrared frequencies observed in the region 2300–600 cm^{-1} for all four complexes are given in Table II. Only the peaks of interest are noted. The single-crystal electronic spectra of $[Me_4N]_2[Ni(mnt)_2]$ in the region 16 700–29 400 cm^{-1} at various temperatures ranging from 19 to 298 K are shown in Figure 3a. At room temperature a broad band envelope was observed with six peaks. As the crystal was cooled, the overall band intensity decreases, accompanied by an increase in resolution. At 19 K, maximum resolution was observed, showing at least 10 peaks in this region. The peak positions and the relative intensities at room temperature are given in Table III. A weak band, which is not listed in Table III, was observed at room temperature centered at about 12 000 cm^{-1}. The single-crystal EPR spectrum of the

(21) The standard values of binding energy for atoms quoted in the Operation Manual for the VG ESCA MarkII spectrometer.

Table III. Electronic Spectra of $[Me_4N]_2[Ni(mnt)_2]$ at 19 and 298 K and $[n\text{-}Bu_4N]_2[Ni(mnt)_2]$ at 50 K and Assignments of the Transitions

band max obsd, cm^{-1}			
$[Me_4N]_2[Ni(mnt)_2]$		$[n\text{-}Bu_4N]_2[Ni(mnt)_2]$	
298 K	19 K	50 K	assignment
18 940 (740)[a]	18 870	18 020	$^1A_g \rightarrow {}^1B_{2g}$ ($yz \rightarrow xy$)
	19 080	18 420	
	19 610	18 800	$^1A_g \rightarrow {}^1B_{1g}$ ($z^2 \rightarrow xy$)
	19 960	19 200	
20 230 (1270)	20 160	19 880	$^1A_g \rightarrow {}^1B_{3g}$ ($xz \rightarrow xy$)
	20 530	20 320	
	21 100	21 050	
21 680 (1660)	21 690	21 270	$^1A_g \rightarrow {}^1B_{2u}$ ($xz \rightarrow a_u$)
	22 370	22 270	$^1A_g \rightarrow {}^1B_{3u}$ ($yz \rightarrow a_u$)
	23 150	23 040	
22 980 (860)	23 810	23 580	$^1A_g \rightarrow {}^1B_{3u}$ ($b_{3u} \rightarrow xy$)
23 780 (220)	24 270	24 390	
26 920 (5260)	26 320	26 570	$^1A_g \rightarrow {}^1B_{1g}$ ($n_{=s:} \rightarrow M$)
	27 620	27 320	$^1A_g \rightarrow {}^1B_{2u}$ ($b_{2u} \rightarrow xy$)

[a] The band intensities are given in parentheses in arbitrary units.

Cu(II) doped in $[n\text{-}Bu_4N]_2[Ni(mnt)_2]$ at 20, 50, and 300 K at a selected orientation is shown in Figure 4. It can be seen that there are eight lines in the spectrum at 300 K due to the isotopes ^{63}Cu and ^{65}Cu. Each of these lines split into two at 50 K and into three at 20 K. This ESR spectral characteristic is reversible on increasing the temperature. Raman spectra of the single crystal in the range 20–600 cm^{-1} at 30 and 300 K are shown in Figure 5. At room temperature one strong peak at 25 cm^{-1} with two shoulders at 37 and 61 cm^{-1} and four low-intensity bands at 130, 182, 278, and 505 cm^{-1} were observed. The overlapping band structure below 100 cm^{-1} has resolved into three peaks centered at 32, 47, and 61 cm^{-1} at 30 K. The bands observed at 130, 182, and 505 cm^{-1} have split into two each, with a separation of 10–25 cm^{-1}, and peak heights have a general increase accompanied by narrowing at 30 K.

Discussion

We refer to the four complexes $[Me_4N]_2[Ni(mnt)_2]$, $[n\text{-}Bu_4N]_2[Ni(mnt)_2]$, $[Me_4N][Ni(mnt)_2]$, and $[n\text{-}Bu_4N][Ni(mnt)_2]$ as A, B, C, and D respectively for convenience. From our experimental data, we are able to identify three or four peaks for C(1s) (apart from the C(1s) peak from the pump oil) and two peaks for N(1s) corresponding to the complex. Considering the chemical equivalence of the carbon and nitrogen atoms, we have labeled them as shown in Figure 6. In the case of B and D there will be four inequivalent carbon atoms while in A and C there will be only three types and C(4) will be absent. In the case of A and B there will be two cations for every complex anion, but this is not shown in the figure. From the experimentally obtained binding energies the shifts from the standard values have been calculated and these are given in Table I. There is an increase in ΔE of Ni going from A → C and B → D, respectively, i.e., the BE shift on Ni seems to reflect directly on the change in its formal oxidation state. The tetrabutylammonium complexes show a relatively higher ΔE_{Ni} compared to the tetramethylammonium complexes. However, in the case of ΔE_S, there is a large difference between the diamagnetic complexes A and B though there is no difference of ΔE_S in the paramagnetic systems. While ΔE_S becomes less negative going from A → C, it becomes more negative going from B → D. From these data it can be inferred that B

Table IV. Charges Obtained in $R_n[Ni(mnt)_2]$ Complexes by Larsson's Equations

	charges							
compd	Ni	S	C(1)	C(2)	C(3)	C(4)	N(1)	N(2)
$[Me_4N]_2[Ni(mnt)_2]$ (A)	0.70	−0.27	−0.04	0.24	0.12		−0.13	0.39
$[n\text{-}Bu_4N]_2[Ni(mnt)_2]$ (B)	0.78	0.03	0.00	0.24	0.17	0.09	−0.11	0.33
$[Me_4N][Ni(mnt)_2]$ (C)	0.77	−0.06	−0.02	0.24	0.12		−0.20	0.23
$[n\text{-}Bu_4N][Ni(mnt)_2]$ (D)	0.90	−0.06	−0.06	0.22	0.10	0.03	−0.20	0.29

Table V. Charges Obtained for $R_n[Ni(mnt)_2]$ Complexes

	charges from (4)							
compd	Ni	S	C(1)	C(2)	C(3)	C(4)	N(1)	N(2)
$[Me_4N]_2[Ni(mnt)_2]$ (A)	0.21	−0.25	−0.08	0.19	0.08		−0.20	0.43
$[n\text{-}Bu_4N]_2[Ni(mnt)_2]$ (B)	0.19	−0.13	−0.07	0.18	0.09	−0.02	−0.19	0.34
$[Me_4N][Ni(mnt)_2]$ (C)	0.21	−0.08	−0.07	0.18	0.06		−0.20	0.20
$[n\text{-}Bu_4N][Ni(mnt)_2]$ (D)	0.25	−0.06	−0.12	0.17	0.05	0.01	−0.18	0.20
	charges from Xα calculations[6]				
complex ion	Ni	S	C(1)	C(2)	N(1)
$[Ni(mnt)_2]^{2-}$	0.276	−0.149	−0.194	0.302	−0.528
$[Ni(mnt)_2]^{-}$	0.271	−0.017	−0.168	0.295	−0.429

has a charge distribution different from that of the other complexes. The same anomalous trend in BE shifts is seen in the case of C(1) as well. The ΔE_C on C(1) is negative in all the complexes except in B, while the ΔE_C on C(2) is nearly the same in all the four complexes. It can be seen that the ΔE_C in C(3) is the same going from A → C whereas it becomes less positive going from B → D. ΔE_C on C(4) is more positive in B than in D The ligand nitrogen atoms seem to be unaffected due to the cation while it becomes more negative as the formal oxidation state of the central metal atom increases. However, ΔE_N in N(2) seems to be affected by a change in the formal oxidation state of the metal as well as the counterion. This anomaly in BE shifts on the atoms in B could therefore be due to a different charge distribution on this complex. Considering the anion, one would expect a positive charge on Ni and C(2) and a negative charge on S, C(1), and N(1).[6] The charges calculated by using Larsson's k values are given for the different atoms in Table IV. Table V shows the charges calculated from (4) as well as those obtained from the Xα calculation.[6] Since the charges have been calculated by DV–Xα (using the simplest approximation) for the anion alone without considering any cation, the charges thus obtained cannot be expected to be very close to those obtained from (4), especially in the cases of C(1), C(2), and N(1). The trend in the charges, shown in Table V, on A, C, and D are as expected while that on B show that charges on C(1), C(3), Ni, S, and N(2) are not as expected. This probably throws light on the interaction of the cation with the anion moiety. From Table V it can be seen that for q_{Ni}, there is an increase in it going from B → D while there is no change in going from A → C. In the case of S there is a decrease in q_S going from A → B while the same is nearly constant in C and D. $q_{C(1)}$ is a constant for A and C while it becomes less negative going from D → B. While $q_{C(2)}$ is nearly constant in all four complexes, $q_{C(3)}$ is slightly more positive in B than in the other three complexes. $q_{N(1)}$ is nearly a constant while $q_{N(2)}$ varies a lot in all four complexes. From C → A, it can be seen that $q_{N(2)}$ increase drastically while it does not increase to that extent going from D → B. Considering the charge distribution on all the four complexes, it can be seen that there is a reorganization of charges on B as compared to A due to the interaction of the anion with the cation. This reorganization of charges can be understood by considering the projection of the molecules based on their crystal structures, which are shown in Figures 7–9. The crystal structures for A and B are available.[22,23] While D is isomorphous with the Cu(III) complex,[24] no structure is available for C. Since A and B have similar structures, except for the tail of the butyl chain in B, it is assumed that the structure

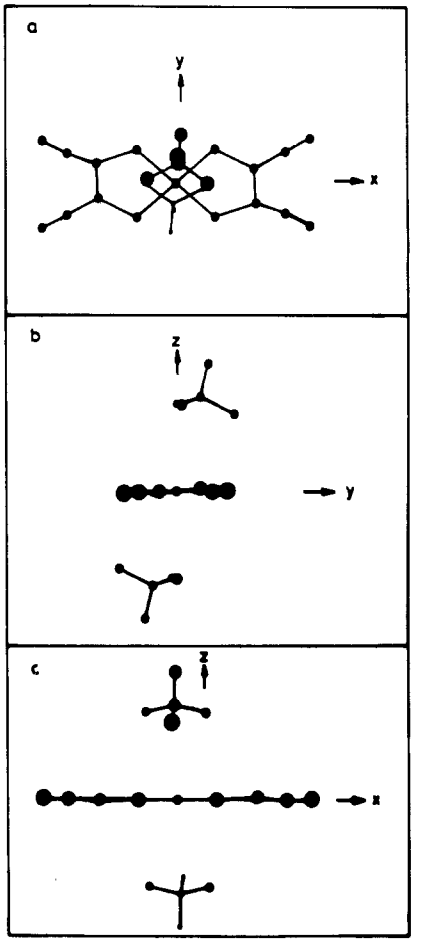

Figure 7. Molecular projections of $[Me_4N]_2[Ni(mnt)_2]$: (a) viewed along the molecular z axis (xy plane); (b) viewed along the molecular y axis (yz plane); (c) viewed along the molecular x axis (xz plane).

Table VI. Interatomic Distances between the Cationic and the Anionic Moieties in $R_n[Ni(mnt)_2]$ Complexes Less Than 4.0 Å

compd	atom pair	dist, Å
$[Me_4N]_2[Ni(mnt)_2]$ (A)	S–C(3)	3.83, 3.99
$[n\text{-}Bu_4N]_2[Ni(mnt)_2]$ (B)	Ni–C(3)	3.8
	S–C(3)	3.96
	C(1)–C(4)	3.52, 3.75
	C(2)–C(4)	3.74, 3.96
$[Me_4N][Ni(mnt)_2]$ (C)	N(1)–C(3)	3.61
$[n\text{-}Bu_4N][Ni(mnt)_2]$ (D)	N(1)–C(3)	3.61
	N(1)–C(4)	3.70, 3.99, 3.66

(22) Kobayashi, A.; Sasaki, Y. *Bull. Chem. Soc. Jpn.* **1977**, *50*, 2650.
(23) Eisenberg, R.; Ibers, J. A. *Inorg. Chem.* **1965**, *4*, 605.
(24) Forrester, J. D.; Zalkin, A.; Templeton, D. H. *Inorg. Chem.* **1964**, *3*, 1507.

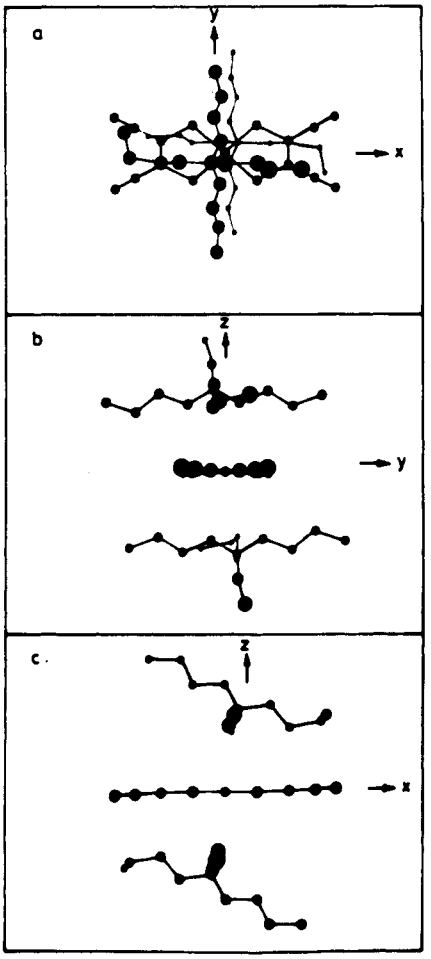

Figure 8. Molecular projections of $[n\text{-}Bu_4N]_2[Ni(mnt)_2]$: (a) viewed along the molecular z axis (xy plane); (b) viewed along the molecular y axis (yz plane); (c) viewed along the molecular x axis (xz plane).

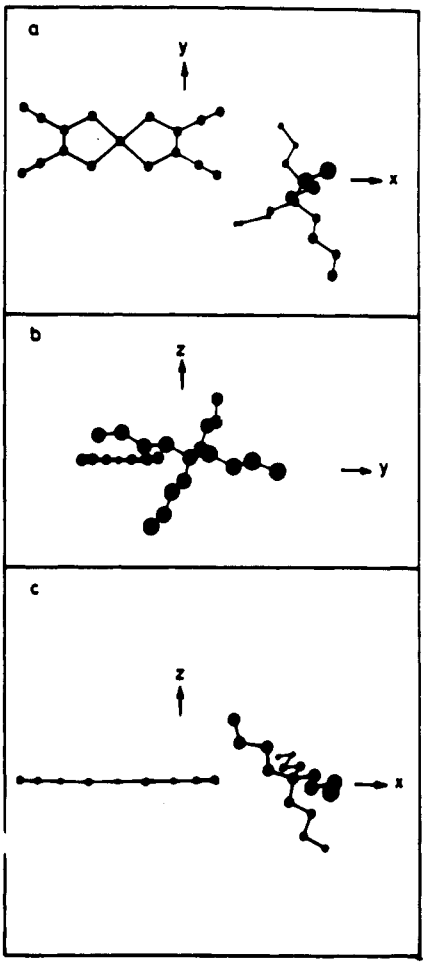

Figure 9. Molecular projections of $[n\text{-}Bu_4N][Ni(mnt)_2]$: (a) viewed along the molecular z axis (xy plane); (b) viewed along the molecular y axis (yz plane); (c) viewed along the molecular x axis (xz plane).

of D can be used for C by cutting off the butyl chain to methyl.

The projections of the molecule in the anionic plane are shown in Figure 7a, 8a, and 9a, and the perpendicular projections are shown in parts b and c of Figures 7–9 for the complexes A, B, and D, respectively. A comparison of these figures reveal that the n-butyl chain extends over the anionic plane passing close to the Ni–S–C(1) angle in B while the counterion is close to the cyano group in both C and D. Calculations of the interatomic distances on each type of atom to all other atoms have been made, and these are presented in Table VI. This reveals that the anion moiety has a considerable interaction with the cation in the case of B. In the case of A and B, the cation is perched on the top of the anionic plane while the cation is on one side of the anion in the case of C and D. However, in B the butyl chain extends over the delocalized π-cloud of the anion while this is not possible in A. Due to the π-cloud present in the complex anion, the charges on the atoms of the counterion in the case of B are affected. Since the N(2) is sufficiently close to the N–S bond and the C(4) bonded to C(3) is close to the C(1) of the ligand, there can be interaction between the cation and the anion leading to a different charge distribution in the case of B.

Further evidence for the charge redistribution in the case of B was obtained from IR spectra of all the four complexes. Since the butyl carbon of the cation is responsible for the anomalous charge distribution in the anion of B, the stretching frequencies ν(C—S) and ν(C=C) and the bending mode π(C—CN)[25] should show an anomalous trend in this complex as compared to the others of this series. In Ni(III) case going from C → D, the ν(C=C) increases from 1482 cm^{-1} by 3 cm^{-1} while in the Ni(II) case ν(C=C) decreases from 1485 cm^{-1} by 4 cm^{-1} going from A to B. In this case π(C–CN) and ν(C–S) + ν(C–C) both show a decrease in going from C → D while both show an increase in going from A → B.

In our efforts to decipher this anomalous behavior of B we have carried out single-crystal electronic spectral studies on complex A at various temperatures down to 19 K. Since the chromophore is basically the $[Ni(mnt)_2]^{2-}$ ion, one would expect a similar electronic spectrum for both A and B. Though it is found to be true in the case of solution spectra (since the ions are solvated), a marked difference has been observed in the crystal spectra even at room temperature. (The spectrum of B is reproduced in Figure 3b from ref 13 for comparison.) (i) There is a shift in some of the peak positions in A compared to those in B. (ii) Though the number of bands must theoretically be the same in A and B because of the same chromophore, the resolution seems to be poor in A and the shape of the band envelope is also slightly different. When the crystal of A is cooled down to 19 K, the overall band intensity in the region 16 670–29 400 cm^{-1} gradually decreases, indicating the orbitally forbidden nature of the transitions in this region. The same behavior was observed for complex B on cooling down to 50 K. However, the difference between these two systems is that, on further cooling to 20 K, B exhibits an increase in intensity[13] while A exhibits a continuous decrease in intensity down to 19 K.

In order to compare the spectra of these two systems, it is desirable to note that all transitions observed in A and B must be the same[13] except for a possible perturbation due to the $[n\text{-}Bu_4N]^+$ cation in B. All the transition energies, their assignments, and a comparison with the transition energies of B[13] are given in Table III. The room-temperature spectrum of A in the region 16 700–29 400 cm^{-1} has been deconvoluted in order to obtain the relative intensities and positions of the peaks. However, from Table

(25) Schlapfer, C. W.; Nakamoto, K. *Inorg. Chem.* **1975**, *14*, 1338.

III, a comparison of the peaks in A at 19 K and B at 50 K (where the maximum resolution was obtained) reveal that the d → d transitions observed in the region 18 500–20 600 cm^{-1} have occurred at higher energies for A than for B. This is in agreement with the charges obtained by ESCA studies. The depletion of charge on sulfur atoms in B causes relatively less ligand field strength. In conclusion, it has become clear by now that the cation influences the charge distribution on the complex anion in B due to its proximity to the π-cloud, whereas this is not possible for the complex A.

This effect of cation on the electronic structure of the complex anion will lead to interesting observations as the system is cooled. At low temperature the thermal motions are restricted, and hence a modification of structure would occur depending upon the resultant molecular structure at that temperature. The electronic spectral studies suggested a distortion in the plane of the complex ion in B below 50 K due to a dihedral angle between the planes of the two ligands attached to the metal.[13] The splitting of EPR lines at 50 and 20 K indicate the formation of two and three magnetically distinct sites, respectively. This is possibly due to the phase transitions of the crystal lattice at these temperatures probably from triclinic (300 K) → monoclinic (50 K) → hexagonal (20 K). The feasibility of this may be found by a closer look into the unit cell dimensions of this crystal at room temperature[23] (a = 12.36 Å, b = 11.138 Å, c = 9.83 Å, α = 118.4°, β = 92.05°, γ = 91.91°). Since the angles β and γ are close to 90°, on cooling, the system can easily transform into a monoclinic cell by grouping four triclinic unit cells. The same logic may be extended to the transformation of a hexagonal cell also since α is close to 120°. However, this requires a large change in the axes b and c. These phase transition may be accompanied by a small distortion in the molecule. A comparison of the Raman spectrum at 300 K with that at 30 K reveals the peaks at 130, 182, and 505 cm^{-1} due to π(ring), δ(C–CN), and δ(C–CN) + ring deformation[25] split into two each on cooling. In addition, an overall increase in the intensity of the bands was observed. This indicates a transformation of the molecule from a centrosymmetric geometry to a noncentrosymmetric geometry. The splitting of lines at 30 K probably indicates two molecular sites. The lines below 100 cm^{-1} are usually due to lattice vibrations, which in this case show a considerable change between the spectra at 30 and 300 K. The increased resolution and the shift of the peaks to low-energy region support the idea of a lattice transformation. A consideration of the monoclinic lattice by grouping four triclinic unit cells would lead to different symmetry properties of the lattice. A minimum of C_2 symmetry exists in the lattice by which the lattice vibrations may be classified under two irreducible representations A and B; hence, considerable shift in their energies may occur. The splitting of the overlapping band structure centerd at 25 cm^{-1} at 30 K can thus be understood as due to a lattice transformation. A detailed investigation into these phase transitions is underway.

Conclusions

A systematic study of photoelectron spectroscopy with the knowledge of interatomic distances enables us to determine the charge distribution in molecules. A general equation for this purpose has been developed. This would also allow one to determine the inter- and intramolecular effects as exemplified by the fact that these studies lend support to the phase transitions observed by other techniques such as infrared, EPR, and Raman spectroscopy. A detailed study on the phase transitions of $[n\text{-}Bu_4]_2[Ni(mnt)_2]$ by a crystal structure determination and EPR studies at low temperatures will reveal the exact geometry and lattice structure of the molecule.

Acknowledgment. We thank the RSIC, IIT, Madras, India, for the experimental facilities and the Department of Science and Technology, Government of India, for funding the project of P.T.M.

Registry No. A, 21584-46-3; B, 18958-57-1; C, 71127-88-3; D, 55401-12-2; carbon, 7440-44-0.

Contribution from the Departments of Chemistry, Smith College, Northampton, Massachusetts 01063, and U.S. Naval Academy, Annapolis, Maryland 21402

Hydrolysis of a Metal-Coordinated Imine by a Proton-Containing Transition State

Tamera K. Cole and R. G. Linck*

Received August 10, 1987

Kinetic studies of the rate of disappearance of $Fe(TIM)(H_2O)_2^{2+}$ are reported. The rate law is first order in the Fe(II) complex, first order in H^+, and independent of the concentration of $Fe(H_2O)_6^{2+}$, with a second-order rate constant of 0.178 ± 0.005 M^{-1} s^{-1} at 25 °C and an ionic strength of 0.5 M. Activation parameters for the reaction were determined to be $\Delta H^{\ddagger}$ = 49.3 ± 0.9 kJ/mol and $\Delta S^{\ddagger}$ = −94 ± 3 J/(mol deg). The presence of CO or CH_3CN in the coordination shell of Fe(II) retards the reaction. This feature allows a determination of the equilibrium constant for the loss of CH_3CN from $Fe(TIM)(CH_3CN)(H_2O)^{2+}$: The value is found to be (2.5 ± 0.5) × 10^{-3}. Spectral measurements indicate that $Fe(TIM)(H_2O)_2^{2+}$ has the same electronic structure as the other iron–TIM complexes and hence is diamagnetic. The mechanism of the reaction is suggested to involve a displacement of the iron ion from the plane of the macrocyclic ring, promoted by a spin change, followed by hydrolysis of the free ligand.

In an earlier paper on the kinetics and equilibria involved in reactions of $Fe(TIM)(CH_3CN)_2^{2+}$ and $Fe(TIM)(CH_3CN)(H_2O)^{2+}$ (where TIM is 2,3,9,10-tetramethyl-1,4,8,11-tetraazacyclotetradeca-1,3,8,10-tetraene) in aqueous CH_3CN solution, it was reported that solutions of the iron complex were unstable in the presence of vanadous ion.[1] Our attempt to explain this curious observation led to further investigation, which is the subject of this report. Herein we show that the mechanism of the reaction is substitution of the diaquo form of the complex ion in the ferrous oxidation state followed by hydrolysis of the imine ligand. The only need for a reducing agent is to ensure the iron ions remain dipositive. The transition state contains the complex ion and a proton. This rate law is unusual if one considers that the complex has no lone pair of electrons available for interaction with the proton. We postulate that an important step of this substitution process involves a spin change of the Fe(II) ion as it moves out of the plane of the ligand, facilitated by the association of the proton with the incipient imine lone pair. A process involving the movement of an iron ion out of the plane of a macrocyclic ligand with attendant spin change was suggested to be important in substitutions in porphyrin chemistry several

* To whom correspondence should be addressed at the U.S. Naval Academy.

(1) Butler, A.; Linck, R. G. *Inorg. Chem.* **1984**, *23*, 2227–2231.

0020-1669/88/1327-1498$01.50/0